Applied Physics Letters ARTICLE pubs.aip.org/aip/apl

High-temperature photon-type ultra-broadband detectors based on ratchet structure

Cite as: Appl. Phys. Lett. **123**, 061112 (2023); doi: 10.1063/5.0153025
Submitted: 4 April 2023 · Accepted: 31 July 2023 ·
Published Online: 9 August 2023

View Online

Export Citation

CrossMark

X. H. Li,[1] S. H. Huang,[1] Q. Yu,[1] X. Yuan,[1] Y. Liu,[1] P. Bai,[2] W. J. Song,[1] H. Z. Bai,[3,4] G. Y. Xu,[3,4] W. Z. Shen,[1] and Y. H. Zhang[1,a)]

AFFILIATIONS

[1]Key Laboratory of Artificial Structures and Quantum Control, School of Physics and Astronomy, Shanghai Jiao Tong University, Shanghai 200240, China
[2]Institute of Applied Physics and Computational Mathematics, Beijing 100088, China
[3]Key Laboratory of Infrared Imaging Materials and Detectors, Shanghai Institute of Technical Physics, Chinese Academy of Sciences, Shanghai 200083, China
[4]Hangzhou Institute for Advanced Study, University of Chinese Academy of Sciences, Hangzhou 310024, China

[a)]Author to whom correspondence should be addressed: yuehzhang@sjtu.edu.cn

ABSTRACT

Achieving a photodetector with high bandwidth, high sensitivity, high speed, and high operating temperature is a common goal for researchers, especially for infrared and terahertz regions due to its important application in various fields like military defense and biochemical analysis. Among photon-type terahertz (THz) detectors, heterojunction interfacial work function internal photoemission (HEIWIP) detectors demonstrate high bandwidth, high sensitivity, and high speed, but are limited by the low operating temperature. In this work, we developed an effective strategy for raising its operating temperature by introducing ratchet structures. By comparing with traditional HEIWIP, the ratchet HEIWIP exhibits a low dark current and high detectivity while retaining the ultra-broad response bandwidth. The operating temperature has been raised from 7 to 20 K in the terahertz region, which is meaningful progress in THz photon-type detection. The universality of this scheme makes it possible to be further migrated to general photon-type semiconductor detectors.

Published under an exclusive license by AIP Publishing. https://doi.org/10.1063/5.0153025

18 February 2024 02:33:51

Over the past two decades, there has been a significant emergence of infrared (IR) and terahertz (THz) detection technologies.[1–3] These technologies have found wide-ranging applications in military defense, agri-food evaluation, and 3D tomography.[4–7] Achieving a high bandwidth photodetector response from IR to THz with high sensitivity, high speed, and high operating temperature has been a common goal among researchers as technology evolves.

Mainstream commercial THz detectors typically rely on the thermal effect. However, due to the thermal mechanism, these detectors have a response time of approximately 10 ms, hindering their application in high-speed sensing.[8] Despite the introduction of advanced materials and antenna structures to enhance the performance of THz detection in recent years, the instability of sample fabrication and incompatibility with existing readout circuits remain the two primary barriers to usage.[9–12]

In contrast, photon-type semiconductor detectors exhibit high sensitivity and high speed in both IR and THz detection.[8,13,14] To accommodate diverse application scenarios, broadband and tunable photodetectors have gained popularity as a prominent research trend in recent years. Due to its maturity as a material, p-type GaAs semiconductors possess multiple absorption mechanisms and are easily fabricated, making them suitable for broadband detection.[15] A recent study reported a heterojunction interfacial work function internal photoemission (HEIWIP) detector based on p-type GaAs, which exhibits an ultra-broadband response covering from 3 to 165 THz with a high responsivity of 7.2 A/W at 9.2 THz. Additionally, the detectivity (D$*$) of HEIWIP typically ranges from 10^9 to 10^{10} cm Hz$^{1/2}$/W, highlighting its potential for high-performance photodetection.[16,17]

Despite its high performance, the practical application of photon-type detectors is hindered by the extremely low operating temperature in the THz region. The primary objective of raising the operating temperature is to enhance sensitivity by improving responsivity and suppressing noise. Methods for increasing the operating temperature can be categorized as either external or internal. A commonly used external method is applying antennas to enhance the optical coupling in the device. Systematic studies of the antenna design

have been proposed for both narrow-band and broadband photon-type detectors.[18,19] On the other hand, developing an effective solution through the proper design of the internal energy band structure holds significant importance. The main idea of the internal method is to suppress the dark current. Resonant tunneling quantum well detectors (RTQWD) and quantum cascade photodetectors (QCDs) are two representative structures.[20,21] Both structures filter dark currents by the tunneling effect. Due to their intrinsic detection mechanism, the response bands of RTQWD and QCD are narrow. Despite being designed for broadband detection, the response window of an InGaAs–InAlAs QCD is still limited.[22] Very recently, the ratchet structure is introduced into ultra-broadband photon-type semiconductor detectors. The low dark current and an optimized NEP of 3.5 $pW/Hz^{1/2}$ at 5 K demonstrate its potential for high-sensitivity and high-temperature detection.[23] The concept of ratchet originates from thermal dynamics and was initially proposed by Feynman in renowned pawl-paddle wheel model.[24] The ratchet structure has a rectifying effect under a non-equilibrium state and effectively blocks the dark current. Due to these unique properties, the ratchet structure holds great potential for increasing the operating temperature of THz detection.

In this work, we propose an efficient method that utilizes the ratchet structure to enhance the operating temperature of photon-type semiconductor detectors in THz detection. We investigate the ultra-broadband response of ratchet HEIWIP using HEIWIP as a representative. Furthermore, the impact of the ratchet structure on suppressing noise is analyzed via the dark current and the background-limited infrared performance temperature (T_{BLIP}). The high-temperature photoresponse spectra of ratchet HEIWIP demonstrate the effectiveness of the ratchet-based method in increasing the operating temperature of photon-type detectors.

The structures of HEIWIP and ratchet HEIWIP are shown in Fig. 1(a). Both devices are grown on semi-insulating GaAs substrates by molecular beam epitaxy. The HEIWIP detector is composed of ten periods of heterojunctions containing a p-$Al_{0.005}Ga_{0.995}As$ emitter layer (500 Å, 3×10^{18} cm^{-3}) and an undoped GaAs barrier layer (2000 Å). The top and bottom contacts are both composed of p-GaAs and doped to 1×10^{19} cm^{-3}. The ratchet HEIWIP consists of ten periods ratchet heterojunctions containing a p-$Al_{0.005}Ga_{0.995}As$ emitter layer (500 Å, 3×10^{18} cm^{-3}) and an undoped asymptotic $Al_xGa_{1-x}As$ barrier layer (1000 Å) sandwiched between two undoped GaAs barriers (500 Å). The Al component of $Al_xGa_{1-x}As$ in the asymptotic potential varies linearly from 0 to 0.07. The top and bottom contacts are both p-GaAs doped to 3.6×10^{18} cm^{-3}, which is slightly decreased to reduce reflectance without affecting the Ohmic contact and comparison. The key difference between ratchet HEIWIP from traditional HEIWIP is the addition of the asymptotic potential in the intrinsic barriers. The samples are processed by wet etching square mesa elements. The bottom and top contact layers are covered by Ti\Pt\Au to ensure good Ohmic contact. It is worth noting that the ratchet embedding strategy in this work differs markedly from previous works, which required to separate ratchets and constant barriers and introduced an offset to trigger the very-long-wavelength infrared (VLWIR) response caused by hot-cold hole energy transfer.[23,25] The presence of four different layers of structures in one period in this design scheme increases the thickness of the device and complicates the growth process. In our design, we simplify the structure by combining the ratchet and constant barriers.

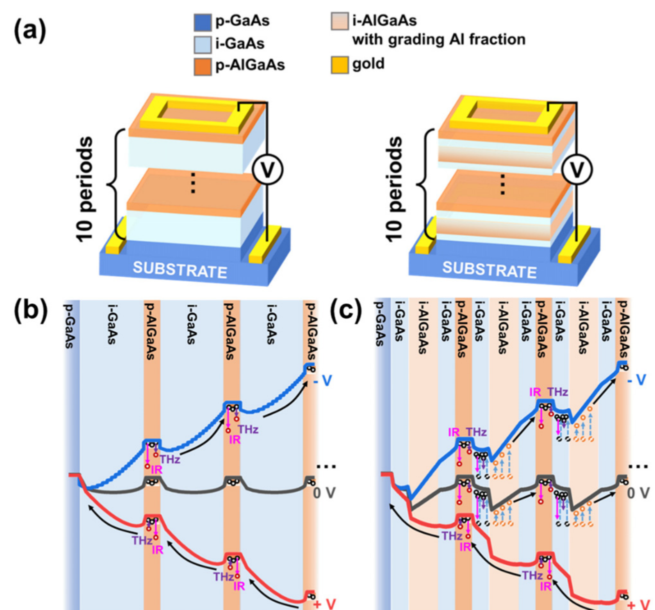

FIG. 1. (a) Device structure of the HEIWIP without and with ratchets. Band diagram and mechanism of the HEIWIP (b) and the ratchet HEIWIP (c). The blue dash arrows represent the relaxation of hot carriers.

The energy band diagrams of HEIWIP and ratchet HEIWIP calculated using a Poisson equation solver under different biases are presented in Figs. 1(b) and 1(c). We define the forward bias with the bottom contact being grounded. It is worth noting that the detection mechanisms of HEIWIP under both forward and reverse biases remain the same due to the spatial inversion symmetry of the energy band. At zero bias, no response is observed. When incident THz/IR light interacts with the highly doped p-$Al_{0.005}Ga_{0.995}As$ emitter layers, holes are excited to higher energy states through intraband free-carrier absorption (FCA) and inter-valence-band absorption (IVBA).[16] Consequently, the free carriers overcome the interfacial work function caused by both the bandgap offset and the band narrowing effect. The response due to FCA is very broad, covering THz to IR regions. The IVBA includes HH–LH band transitions and LH/HH band–SO band transitions (LH stands for the light hole, HH stands for the heavy hole, and SO stands for spin–orbit split-off). The response due to IVBA mainly appears in IR regions.

The introduction of a ratchet structure in HEIWIP breaks the spatial inversion symmetry, resulting in distinct response behaviors of ratchet HEIWIP under forward and reverse biases. Notably, the response can also be observed at zero bias, which is a specific characteristic of the ratchet effect. When a forward bias is applied and the ratchet structure is flattened, the behavior of ratchet HEIWIP resembles that of a traditional HEIWIP detector. At zero bias, carriers are blocked by the heterojunction interfacial barriers and the asymptotic barriers at equilibrium. However, when THz and IR light irradiate the system, carriers absorb energy through FCA and IVBA processes, transitioning to higher energy levels and driving the system into a non-equilibrium state. Subsequently, these carriers redistribute due to diffusion and explore the asymmetric potential landscape. Some

18 February 2024 02:33:51

Published under an exclusive license by AIP Publishing

carriers enter the asymptotic potential zone and move forward during relaxation due to the ratchet potential, which is known as the light-induced ratchet effect.[23,26] Under reverse bias, the ratchets become sharper. In this case, the photocurrent is attributed not only to the light-induced ratchet effect but also to the external bias drive.

The asymmetry band structure leads to the variation in responsivity. The responsivity spectra of traditional HEIWIP and ratchet HEIWIP under different biases at THz and IR regions are shown in Figs. 2(a)–2(d). The photoresponse spectra were obtained using a Brucker VERTEX 70 Fourier transform infrared spectrometer (FTIR) by replacing the internal detector with our devices. The spectra on the THz/MIR region were measured with an HDPE window/a KRS5 window, respectively. The responsivity spectra were calibrated using an Infrared Systems Development Corporation IR-564/301 blackbody, an SR-570 low-noise current preamplifier, and an SR-830 lock-in amplifier. The background photocurrent was measured using a Keithley 2400 source meter. Both devices demonstrate ultra-broadband response from THz (150 cm^{-1}) to SWIR (5000 cm^{-1}), which is mainly attributed to the FCA. The valley between 200 and 300 cm^{-1} refers to the "Reststrahlen band" due to GaAs-like TO phonons, while the valley at 357 cm^{-1} refers to AlAs-like TO phonons. The valleys between 300 and 600 cm^{-1} are attributed to multiple-phonon absorption.[27,28] The peaks at 935, 1310, 1820, and 3050 cm^{-1} are caused by the IVBA including HH–LH band transitions and LH/HH band–SO band transitions.[29] By comparing with the traditional HEIWIP, we can observe zero response in the ratchet HEIWIP, which is a critical feature of the ratchet effect. The peak responsivity of ratchet HEIWIP is 0.19 A/W at 387 cm^{-1} in the THz region and 0.04 A/W at 935 cm^{-1} in the IR region, while that of traditional HEIWIP is 0.38 A/W at 325 cm^{-1} in the THz region and 0.4 A/W at 771 cm^{-1} in the IR region. The decrease in responsivity of ratchet HEIWIP is caused by the block of ratchet barriers. Due to the spatial inversion asymmetry of ratchet structures, the blocking effect under reverse bias is always higher, producing a lower responsivity. In contrast to the conventional HEIWIP, the sensitivity of the ratchet HEIWIP to light at wavenumbers above 450 cm^{-1} is reduced, while the proportion of response in 350–450 cm^{-1} is relatively enhanced. In addition, the decrease in IR responsivity is more significant. To better understand this phenomenon, we need to focus on the microscopic response mechanism in the ratchet HEIWIP, as shown in Figs. 2(e) and 2(f). In traditional HEIWIP, carriers absorb photons through FCA and IVBA. However, in ratchet HEIWIP, the gradient barriers block part of carriers resulting from FCA and IVBA and introduce different absorption mechanisms. Under zero or weak biases, the constant barriers would bend and form a potential valley. The carriers that originally absorb THz and FIR photons to generate current in conventional HEIWIP are now blocked by the gradient barriers in ratchet HEIWIP and relax into the valley region. Due to the accumulation of carriers, the activation energy for carriers in the valley is the difference between the maximum height of the gradient barrier Δ_g and the Fermi energy of relaxed carriers in the valley E_{Fv}, which falls in the THz region. Therefore, part of the carriers resulting from FIR FCA is blocked by the gradient barriers and contributes to THz response, resulting in the change in spectra shape, which is similar to the case of optically pumped absorption.[25] The introduction of the ratchet structure blocks photocurrent in all bandwidth but introduces an extra absorption mechanism in the THz region, making the HEIWIP more sensitive to the low-energy THz light.

Although part of the photocurrent is sacrificed, the suppression of the dark current is more prominent. The I–V characteristic curves

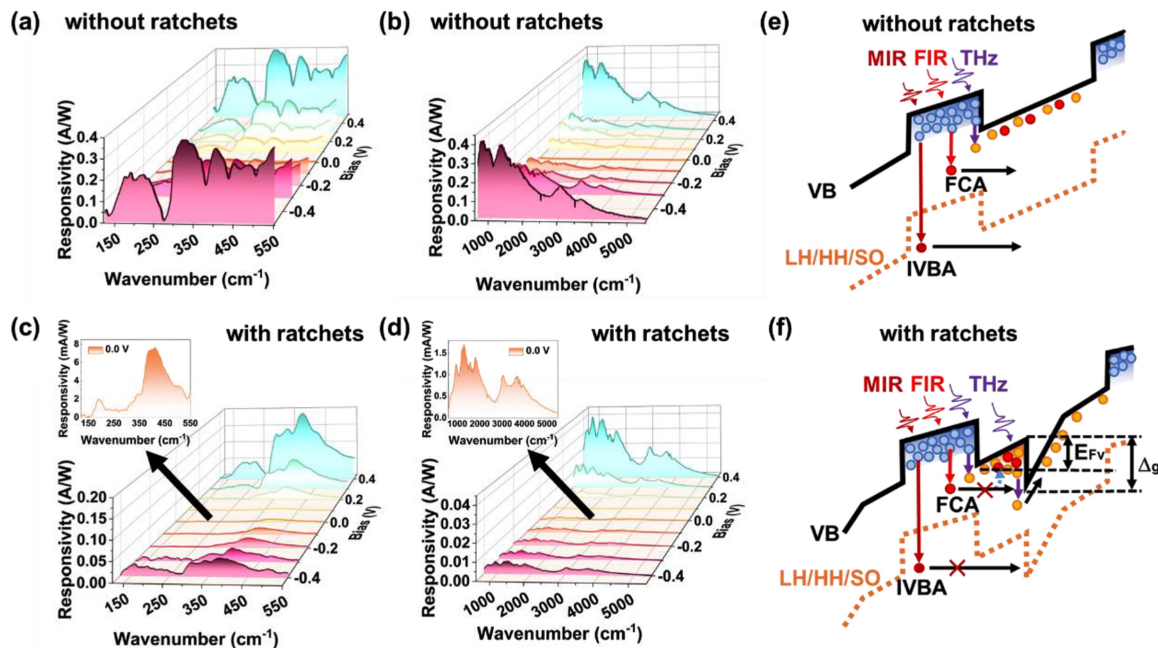

FIG. 2. (a) THz and (b) IR responsivity spectra of the HEIWIP at 7 K under different biases. (c) THz and (d) IR responsivity spectra of the ratchet HEIWIP at 7 K under different biases. The schematic of microscope photoresponse mechanism of the HEIWIP (e) and ratchet HEIWIP (f). The blue dashed arrow represents relaxation.

18 February 2024 02:33:51

Published under an exclusive license by AIP Publishing

under dark conditions and with 300 K background radiation at different temperatures of HEIWIP and ratchet HEIWIP are shown in Figs. 3(a) and 3(b), respectively. The dark condition is measured by a shield cover made of a gold-plated copper lid. By comparing with traditional HEIWIP, the I–V curves of ratchet HEIWIP exhibit obvious asymmetry under low temperature, coinciding with the spatial inversion asymmetry of its energy band structure. Thermally generated carriers spontaneously generate directional movement under a ratchet structure, producing a net current under zero bias. At higher temperatures, the carriers transit to high energy levels more easily due to stronger thermal excitation, and the ratchet effect is shielded. The dark current of traditional HEIWIP is sensitive to the operating temperature and dominates as the temperature approaches 15 K. In contrast, ratchet HEIWIP demonstrates good suppression of dark current up to 25 K. The dark current of ratchet HEIWIP is lower than HEIWIP by 2–5 orders of magnitude. An important metric of the operating temperature is T_{BLIP}, at which the dark current is equivalent to the 300 K background radiation generated photocurrent (i.e., the ratio I_{BG}/I_{DARK} equals 2). As shown in Figs. 3(c) and 3(d), the T_{BLIP} of ratchet HEIWIP is 23 K, while that of HEIWIP is 13 K. As the operating temperature of semiconductor photon type detectors in THz detection is generally liquid helium temperature, the increase by 10 K is significant progress.

The enhancement in operating temperature primarily arises from the suppression of dark current caused by the ratchet effect. As illustrated in the inset of Figs. 3(c) and 3(d), in traditional HEIWIP, the dark current is composed of thermal excitation (TE) current and scattering-assisted tunneling (SAT) current. The carriers in emitters overcome the interfacial barrier through thermal excitation, forming TE current. At a certain bias, the carriers with total energy lower than the potential barrier can tunnel through the barrier tip due to electron and phonon scattering, forming SAT current. As the ratchet structure is thick enough (~0.1 μm) and the applied electric field is low ($\leq 10^3$ V/cm), the tunneling current is negligible. Therefore, the thermal excitation dark current can be described by a 3D drift model, as shown below:[30]

$$I_{\rm dark} = eA\frac{\mu F}{\left[1+\left(\frac{\mu F}{v_{\rm sat}}\right)^2\right]^{\frac{1}{2}}}2\left(m^*\frac{kT}{2\pi\hbar^2}\right)^{\frac{3}{2}}\times\exp\left[-\frac{\Delta_{act}-\alpha F}{kT}\right], \tag{1}$$

where e is the elementary charge, A is the device area, μ is the carrier mobility, F is the applied electric field, v_{sat} is the saturation drift velocity of carriers, m^* is the effective mass, Δ_{act} is the thermal activation energy, generally equals to the difference between interfacial barrier Δ and the Fermi energy E_F in emitters, and α is the coefficient determining the effective barrier lowering (~100–200 Å). In ratchet HEIWIP, carriers need to experience two thermal excitation processes before forming the dark current. Its equivalent thermal activation energy $\Delta_{act} = \Delta + \Delta_g - E_F - FL_{cb}$, where Δ_g is the maximum height of the $Al_xGa_{1-x}As$ gradient barrier, and L_{cb} is the width of the constant barrier formed by intrinsic GaAs. Under a low electric field, the inclination of the constant barrier is small compared with the gradient barrier. Therefore, the higher thermal activation energy leads to an obvious suppression of dark current.

The substantial suppression of dark current in ratchet HEIWIP also results in a high detectivity, as shown in Fig. 4. The detectivity $D^* = \frac{A^{1/2}}{NEP}$, where A is the device mesa area and NEP is the noise

18 February 2024 02:33:51

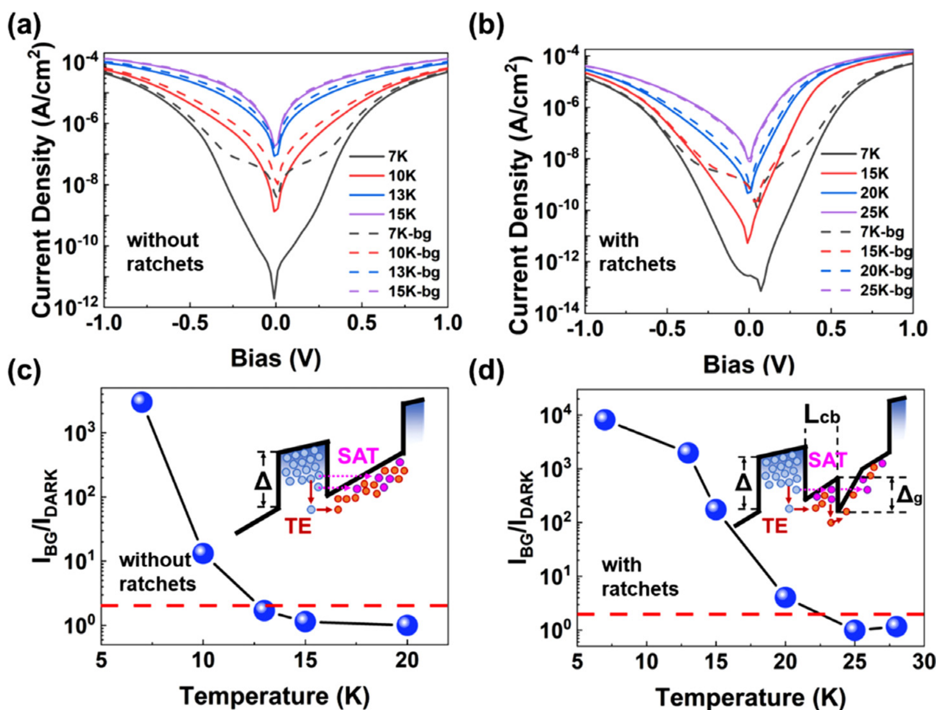

FIG. 3. The I–V characteristic curves under dark conditions (solid) and with 300 K background radiation (dash) at different temperatures of (a) traditional HEIWIP and (b) ratchet HEIWIP. The BLIP temperature of (c) traditional HEIWIP and (d) ratchet HEIWIP. The schematics of the dark current generation mechanism are shown in the insets.

Published under an exclusive license by AIP Publishing

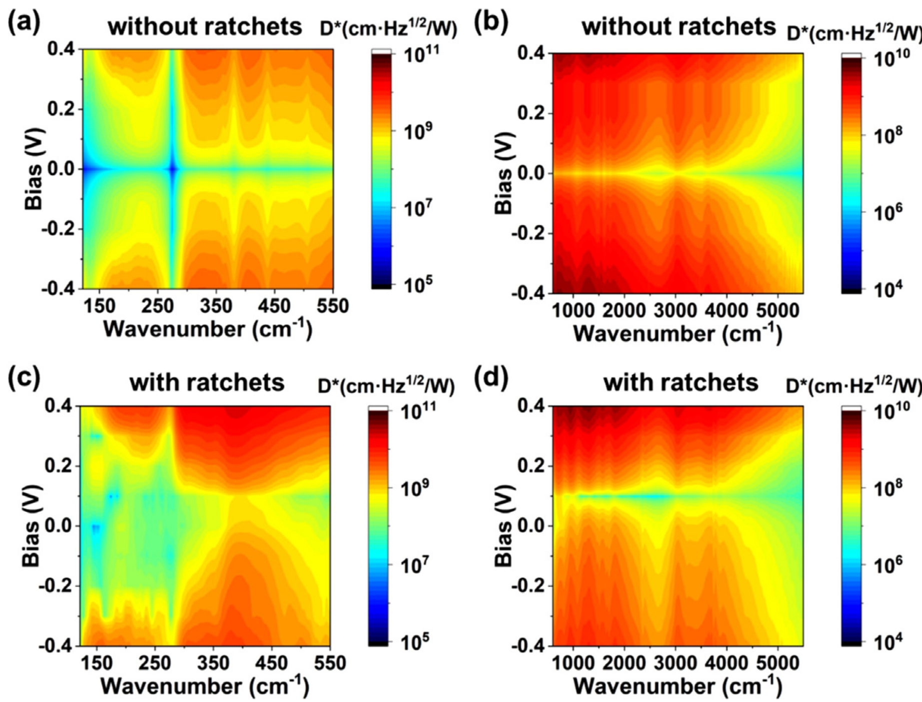

FIG. 4. (a) THz and (b) IR detectivity at 7 K under different biases of traditional HEIWIP. (c) THz and (d) IR detectivity at 7 K under different biases of ratchet HEIWIP.

18 February 2024 02:33:51

equivalent power derived as $NEP = \frac{\sqrt{4ei_d g\Delta f}}{R}$. Here, e is the elementary charge, i_d is current measured under dark radiation, g is the gain of the device, Δf is system measurement bandwidth, and R is the responsivity.[31] The introduction of the ratchet structure gives rise to an observable asymmetry characteristic in the D^*-bias mapping. The ratchet HEIWIP demonstrates a higher detectivity under forward biases compared to traditional HEIWIP. In the THz region, the overall detectivity of ratchet HEIWIP is enhanced by ten times compared with traditional HEIWIP due to the effective suppression of dark current. In the IR region, the detectivity of ratchet HEIWIP is lower due to the ratchet structures, which transform part of the IR response to low energy THz response. The maximum detectivity of ratchet HEIWIP attains 2.5×10^{10} cm $Hz^{1/2}$/W at 390 cm^{-1} in the THz region and 5.3×10^9 cm $Hz^{1/2}$/W at 937 cm^{-1} in the IR region. The high detectivity makes it possible for ratchet HEIWIP to work under higher temperatures.

The normalized photoresponse spectra of traditional HEIWIP and ratchet HEIWIP are shown in Fig. 5. The response of traditional HEIWIP from THz to SWIR can hardly be observed at temperatures higher than 8 K. In comparison, we have measured the photoresponse spectra of ratchet HEIWIP up to 20 K in the THz region and 28 K in the IR region. The cutoff frequency shows a slight blue shift, due to the higher thermal excitation energy. A similar phenomenon has also been observed in IR HEIWIPs.[32] The featured peak positions demonstrate similar shifts due to the band offsets between GaAs barriers and AlGaAs emitters enlarging under higher temperatures.

In conclusion, we propose a high-temperature THz/IR photon-type detector based on ratchet structures. As shown in Table I, the ratchet-HEIWIP demonstrates an ultra-high response bandwidth

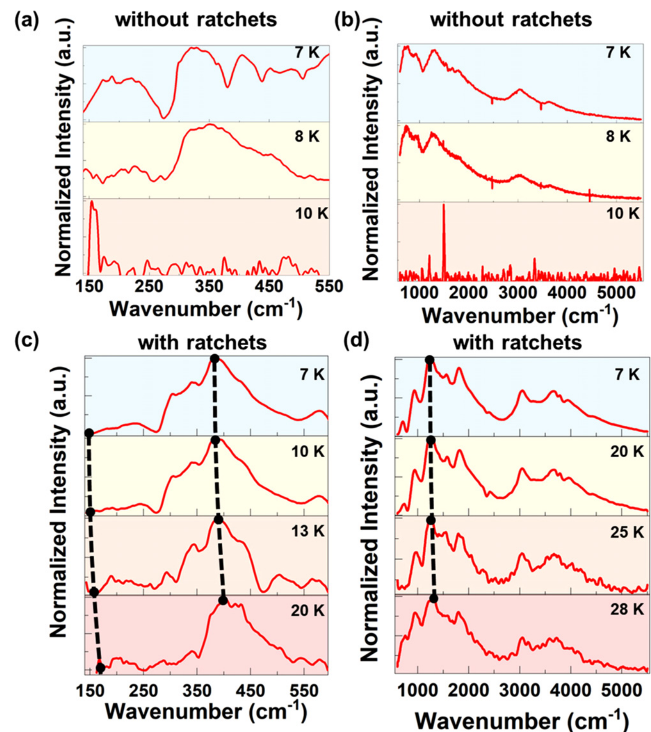

FIG. 5. (a) THz and (b) MIR normalized response spectra of the traditional HEIWIP at higher temperatures. (c) THz and (d) MIR normalized response spectra of the ratchet HEIWIP at higher temperatures.

Published under an exclusive license by AIP Publishing

TABLE I. Comparison between the ratchet-HEIWIP and the state-of-the-art THz photon-type photodetectors.

Detector	Frequency range (THz)	Peak responsivity (A/W)	T (K)	D^* (cm $Hz^{1/2}$/W)
QWP[33]	5	0.5	5	2.5×10^{10}
QDIP[34]	4–15	0.45	4.6	1×10^{8}
QCD[35]	3.5	8.6×10^{-3}	10	5×10^{7}
HIWIP[36]	4–20	6.8	5	2.3×10^{10}
HEIWIP	4.5–150	0.38	8	5.1×10^{9}
Ratchet-HEIWIP	4.5–150	0.19	20	2.5×10^{10}

spanning from THz to SWIR thanks to the diverse detection mechanisms enabled by p-type semiconductors. Moreover, with its high detectivity, the ratchet HEIWIP achieves an operating temperature of 20 K in the THz region. Notably, the ratchet HEIWIP strikes a balance between multiple metrics without the need for external optical coupling structures. Additionally, its inherent short carrier lifetime makes it a promising choice for high-speed THz/IR detection. Beyond its application as a high-speed, high-temperature THz/IR photon-type detector, this work introduces an alternative ratchet embedding method. This approach has the potential to be applied to general THz and IR photon detection.

This work was supported by the Natural Science Foundation of China (Nos. 12274285, 12074249, 61974151, and 62235010).

AUTHOR DECLARATIONS

Conflict of Interest

The authors have no conflicts to disclose.

Author Contributions

Xiaohong Li and Siheng Huang contributed equally to this work.

Xiaohong Li: Conceptualization (equal); Data curation (lead); Formal analysis (lead); Investigation (lead); Methodology (equal); Visualization (lead); Writing – original draft (lead); Writing – review & editing (equal). **Wenzhong Shen:** Funding acquisition (supporting). **Yueheng Zhang:** Conceptualization (lead); Formal analysis (equal); Funding acquisition (lead); Project administration (lead); Writing – review & editing (lead). **Siheng Huang:** Investigation (equal). **Quan Yu:** Investigation (equal). **Xin Yuan:** Investigation (equal). **Ying Liu:** Investigation (equal). **Peng Bai:** Conceptualization (supporting); Writing – review & editing (supporting). **Wenjun Song:** Writing – review & editing (supporting). **Hongzhou Bai:** Methodology (equal). **Gangyi Xu:** Writing – review & editing (equal).

DATA AVAILABILITY

The data that support the findings of this study are available from the corresponding author upon reasonable request.

REFERENCES

[1] M. G. Hauser and E. Dwek, Annu. Rev. Astron. Astrophys. **39**, 249 (2001).
[2] L. M. Miller and P. Dumas, Curr. Opin. Struct. Biol. **20**(5), 649 (2010).
[3] O. A. Smolyanskaya, N. V. Chernomyrdin, A. A. Konovko, K. I. Zaytsev, I. A. Ozheredov, O. P. Cherkasova, M. M. Nazarov, J. P. Guillet, S. A. Kozlov, Y. V. Kistenev, J. L. Coutaz, P. Mounaix, V. L. Vaks, J. H. Son, H. Cheon, V. P. Wallace, Y. Feldman, I. Popov, A. N. Yaroslaysky, A. P. Shkurinov, and V. V. Tuchin, Prog. Quantum Electron. **62**, 1 (2018).
[4] R. M. Smith and M. A. Arnold, Appl. Spectrosc. Rev. **46**(8), 636 (2011).
[5] W. Zhang, Y. Tang, A. R. Shi, L. R. Bao, Y. Shen, R. Q. Shen, and Y. H. Ye, Materials **11**(8), 1364 (2018).
[6] K. Q. Wang, D. W. Sun, and H. B. Pu, Trends Food Sci. Technol. **67**, 93 (2017).
[7] B. Ferguson, S. H. Wang, D. Gray, D. Abbot, and X. C. Zhang, Opt. Lett. **27**(15), 1312 (2002).
[8] F. Sizov, Semicond. Sci. Technol. **33**(12), 123001 (2018).
[9] S. Bevilacqua and S. Cherednichenko, IEEE Trans. Terahertz Sci. Technol. **4**(6), 653 (2014).
[10] I. Kasalynas, R. Venckevicius, L. Minkevicius, A. Sesek, F. Wahaia, V. Tamosiunas, B. Voisiat, D. Seliuta, G. Valusis, A. Svigelj, and J. Trontelj, Sensors **16**(4), 432 (2016).
[11] Y. Z. Zhang, T. Liu, B. Meng, X. H. Li, G. Z. Liang, X. N. Hu, and Q. J. Wang, Nat. Commun. **4**, 1811 (2013).
[12] L. Viti, J. Hu, D. Coquillat, A. Politano, W. Knap, and M. S. Vitiello, Sci. Rep. **6**, 20474 (2016).
[13] A. Poglitsch, C. Waelkens, N. Geis, H. Feuchtgruber, B. Vandenbussche, L. Rodriguez, O. Krause, E. Renotte, C. van Hoof, P. Saraceno, J. Cepa, F. Kerschbaum, P. Agnèse, B. Ali, B. Altieri, P. Andreani, J. L. Augueres, Z. Balog, L. Barl, O. H. Bauer, N. Belbachir, M. Benedettini, N. Billot, O. Boulade, H. Bischof, J. Blommaert, E. Callut, C. Cara, R. Cerulli, D. Cesarsky, A. Contursi, Y. Creten, W. De Meester, V. Doublier, E. Doumayrou, L. Duband, K. Exter, R. Genzel, J. M. Gillis, U. Grözinger, T. Henning, J. Herreros, R. Huygen, M. Inguscio, G. Jakob, C. Jamar, C. Jean, J. de Jong, R. Katterloher, C. Kiss, U. Klaas, D. Lemke, D. Lutz, S. Madden, B. Marquet, J. Martignac, A. Mazy, P. Merken, F. Montfort, L. Morbidelli, T. Müller, M. Nielbock, K. Okumura, R. Orfei, R. Ottensamer, S. Pezzuto, P. Popesso, J. Putzeys, S. Regibo, V. Reveret, P. Royer, M. Sauvage, J. Schreiber, J. Stegmaier, D. Schmitt, J. Schubert, E. Sturm, M. Thiel, G. Tofani, R. Vavrek, M. Wetzstein, E. Wieprecht, and E. Wiezorrek, Astron. Astrophys. **518**, L2 (2010).
[14] H. Li, W. J. Wan, Z. Y. Tan, Z. L. Fu, H. X. Wang, T. Zhou, Z. P. Li, C. Wang, X. G. Guo, and J. C. Cao, Sci. Rep. **7**, 3452 (2017).
[15] A. G. U. Perera, Prog. Quantum Electron. **48**, 1 (2016).
[16] X. H. Li, S. H. Huang, H. Z. Bai, P. Bai, X. R. Lian, W. J. Song, W. Z. Shen, G. Y. Xu, and Y. H. Zhang, Appl. Phys. Lett. **121**(5), 051106 (2022).
[17] S. G. Matsik, M. B. M. Rinzan, A. G. U. Perera, H. C. Liu, Z. R. Wasilewski, and M. Buchanan, Appl. Phys. Lett. **82**(1), 139 (2003).
[18] X. Bai, P. Bai, X. Li, S. Huang, X. Lian, W. Song, Z. Shi, W. Shen, and Y. Zhang, J. Appl. Phys. **130**(20), 203102 (2021).
[19] X. R. Lian, K. Wang, X. Q. Bai, P. Bai, X. H. Li, S. H. Huang, W. J. Song, W. Z. Shen, G. Y. Xu, and Y. H. Zhang, J. Phys. D: Appl. Phys. **55**(47), 475101 (2022).
[20] X. H. Su, S. Chakrabarti, P. Bhattacharya, G. Ariyawansa, and A. G. U. Perera, IEEE J. Quantum Electron. **41**(7), 974 (2005).
[21] F. R. Giorgetta, E. Baumann, M. Graf, Q. K. Yang, C. Manz, K. Kohler, H. E. Beere, D. A. Ritchie, E. Linfield, A. G. Davies, Y. Fedoryshyn, H. Jackel, M. Fischer, J. Faist, and D. Hofstetter, IEEE J. Quantum Electron. **45**(8), 1039 (2009).
[22] D. Hofstetter, F. R. Giorgetta, E. Baumann, Q. Yang, C. Manz, and K. Köhler, Appl. Phys. Lett. **93**(22), 221106 (2008).
[23] P. Bai, X. H. Li, N. Yang, W. D. Chu, X. Q. Bai, S. H. Huang, Y. H. Zhang, W. Z. Shen, Z. L. Fu, D. X. Shao, Z. Y. Tan, H. Li, J. C. Cao, L. H. Li, E. H. Linfield, Y. Xie, and Z. R. Zhao, Sci. Adv. **8**(21), eabn2031 (2022).
[24] A. M. Song, A. Lorke, A. Kriele, J. P. Kotthaus, W. Wegscheider, and M. Bichler, Phys. Rev. Lett. **80**(17), 3831 (1998).
[25] Y. F. Lao, A. G. U. Perera, L. H. Li, S. P. Khanna, E. H. Linfield, and H. C. Liu, Nat. Photonics **8**(5), 412 (2014).
[26] B. Lau and O. Kedem, J. Chem. Phys. **152**(20), 200901 (2020).
[27] J. S. Blakemore, J. Appl. Phys. **53**(10), R123 (1982).
[28] Y. F. Lao, A. G. U. Perera, H. L. Wang, J. H. Zhao, Y. J. Jin, and D. H. Zhang, J. Appl. Phys. **119**(10), 105304 (2016).

18 February 2024 02:33:51

Published under an exclusive license by AIP Publishing

[29]Y. F. Lao, P. K. D. D. P. Pitigala, A. G. U. Perera, H. C. Liu, M. Buchanan, Z. R. Wasilewski, K. K. Choi, and P. Wijewarnasuriya, Appl. Phys. Lett. **97**(9), 091104 (2010).
[30]D. G. Esaev, M. B. M. Rinzan, S. G. Matsik, and A. G. U. Perera, J. Appl. Phys. **96**(8), 4588 (2004).
[31]Y. Yang, H. C. Liu, M. R. Hao, and W. Z. Shen, J. Appl. Phys. **110**(7), 074501 (2011).
[32]Y. F. Lao and A. G. U. Perera, Phys. Rev. B **86**(19), 195315 (2012).
[33]D. Palaferri, Y. Todorov, Y. N. Chen, J. Madeo, A. Vasanelli, L. H. Li, A. G. Davies, E. H. Linfield, and C. Sirtori, Appl. Phys. Lett. **106**(16), 161102 (2015).
[34]X. H. Su, J. Yang, P. Bhattacharya, G. Ariyawansa, and A. G. U. Perera, Appl. Phys. Lett. **89**(3), 031117 (2006).
[35]M. Graf, G. Scalari, D. Hofstetter, J. Faist, H. Beere, E. Linfield, D. Ritchie, and G. Davies, Appl. Phys. Lett. **84**(4), 475 (2004).
[36]P. Bai, Y. H. Zhang, X. G. Guo, Z. L. Fu, J. C. Cao, and W. Z. Shen, Appl. Phys. Lett. **113**(24), 241102 (2018).

18 February 2024 02:33:51

Published under an exclusive license by AIP Publishing